

A Simple Route to Aqueous Suspensions of Degradable Copolymer Nanoparticles from Radical Ring-Opening Polymerization-Induced Self-Assembly (rROPISA)

*Chen Zhu, Stéphanie Denis, Julien Nicolas**

Université Paris-Saclay, CNRS, Institut Galien Paris-Saclay, 92296 Châtenay-

Malabry, France

*To whom correspondence should be addressed.

Email: julien.nicolas@u-psud.fr

Tel.: +33 1 46 83 58 53

Abstract

Degradable polymer nanoparticles are almost exclusively obtained by formulation of preformed degradable polymers, such as aliphatic polyesters, thus resulting in very low nanoparticle concentrations and limited structural diversity. On the other hand, many different vinyl polymers can be obtained by polymerization in aqueous dispersed media, but their non-degradability limits their use especially in the biomedical field. Herein, we combined the best of both worlds by developing a two-step radical ring-opening copolymerization-induced self-assembly (rROPISA) process, allowing to generate aqueous suspensions of narrowly dispersed, degradable vinyl copolymer nanoparticles at 15 wt.% solid contents, containing cyclic ketene acetal (CKA) units in the nanoparticle core. This strategy relied on rROPISA in DMF, followed by a simple transfer step to water. It was successfully applied to the three main CKAs used in rROP and yielded nanoparticles of ~80–215 nm in diameter with tunable amount of CKA up to 21 mol.%. Successful incorporation of ester groups in the copolymers was demonstrated by hydrolytic degradation of both the copolymers and the nanoparticles. The nanoparticles' cytocompatibility was then established by cell viability assays and cell morphology observation with three representative healthy cell lines. Not only this synthetic strategy could be of great potential for drug delivery applications, but it can also be beneficial to other research fields to yield more environmentally friendly materials involving the use of latexes, such as paints or coatings.

1. Introduction

Formulation of aqueous suspensions of degradable polymer nanoparticles has gained tremendous interest notably in the biomedical field.^[1–4] Nanoparticles based on aliphatic polyesters are still considered to be the gold standard given their biodegradability and their FDA-approval for use in humans. However, polyester nanoparticles are exclusively obtained by formulation of preformed polymers using organic solvents because of the impossibility to perform their synthesis in water-borne conditions. It therefore results in very low concentrations in nanoparticles (ca 1–5 wt.%), which limits their use.^[3] Moreover, polyesters also exhibit strong limitations in terms of structural variation, functionalization and regarding the possibility to make sophisticated architectures.

Conversely, vinyl polymers synthesized by reversible deactivation radical polymerization (RDRP) exhibit high structural diversity, ease of functionalization and can be obtained in aqueous dispersed media to produce polymer (nano)particles. However, their non-degradability restricts their use for most biomedical applications because their lack of metabolization and/or excretion^[4] can potentially lead to toxic accumulation of foreign materials in the body. Despite recent developments in radical ring-opening copolymerization (rROP) of cyclic ketene acetals (CKAs),^[5–7] which is the most efficient strategy to insert ester groups in the backbone of vinyl polymers, the preparation of aqueous suspensions of degradable nanoparticles by rROP is still at its infancy.^[8] Therefore, a robust yet simple polymerization process able to produce aqueous suspensions of degradable polyester-like particles is still an unmet need. Such

materials would indeed represent an important addition to the somewhat limited arsenal of degradable polymer nanoparticles available for biomedical applications and open new perspectives regarding environmentally friendly materials.

Among the different polymerization processes in dispersed media, polymerization-induced self-assembly (PISA)^[9–11] has established as the most versatile and robust to generate a wide range of different diblock copolymer nano-object suspensions (e.g., spheres,^[12] vesicles^[13–15] or worms^[16]) without surfactant and with high solids contents (ca 10–50 wt.%). PISA has indeed shown extraordinary flexibility in terms of polymerization techniques and conditions used,^[17–20] monomers polymerized,^[16,21–24] stimuli-responsiveness^[23,25–28] or potential applications. However, even though PISA-derived nano-objects have been suggested for drug delivery or other biomedical applications,^[12,21,29–35] there is yet no strategy to achieve aqueous suspension of degradable, polyester-like nanoparticles by PISA. Conversely, PISA was recently successfully applied to the synthesis of synthetic polypeptide nanoparticles by NCA polymerization.^[36]

Herein, we tackled these challenges by developing a simple, yet robust two-step approach to generate aqueous suspensions of degradable polyester-like nanoparticles by PISA. To do so, we built on our recently developed rROPISA process,^[37,38] a combination between PISA and rROP that served to produce nanoparticles in non-polar solvents. In the present work, the rROPISA process was redesigned to make it fully compatible with the preparation of aqueous suspensions of degradable diblock copolymer nanoparticles (Figure 1). To demonstrate the flexibility of this process, it

was successfully applied to the three main CKAs used in rROP; namely 2-methylene-4-phenyl-1,3-dioxolane (MPDL), 5,6-benzo-2-methylene-1,3-dioxepane (BMDO) and 2-methylene-1,3-dioxepane (MDO). Also, by a careful selection of the different polymer blocks, not only the nanoparticles exhibited a biocompatible shell,^[39–43] but they also showed excellent cytocompatibility on representative healthy human cells.

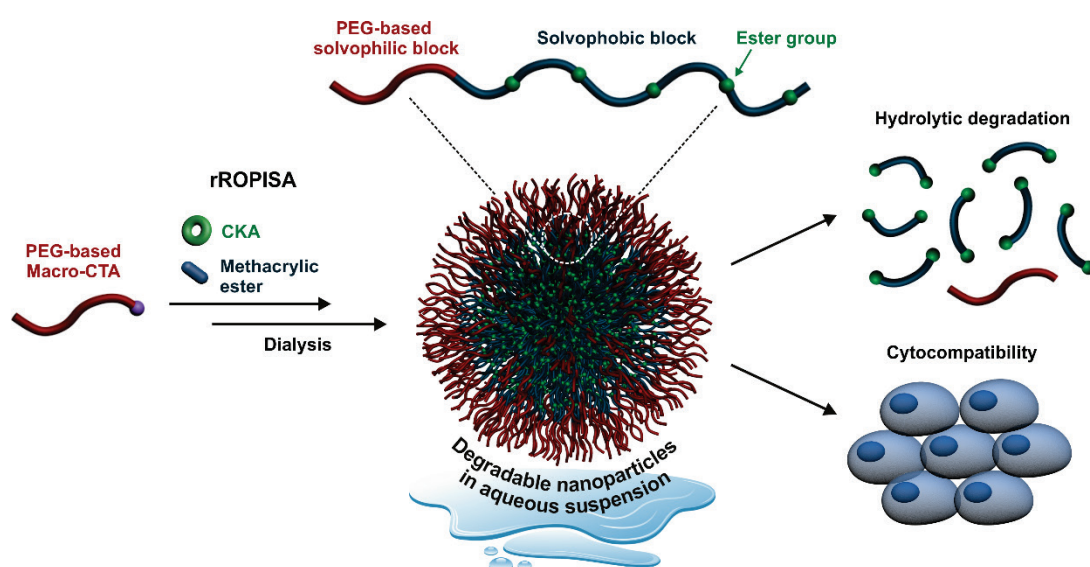


Figure 1. Synthesis of aqueous suspensions of core-degradable diblock copolymer nanoparticles by consecutive radical ring-opening copolymerization-induced self-assembly (rROPISA) from cyclic ketene acetals (CKAs), followed by transfer to water.

2. Materials and Methods

2.1. Materials

Lauryl methacrylate (LMA, 96%) and oligo(ethylene glycol) methyl ether methacrylate (OEGMA, $M_n = 300 \text{ g.mol}^{-1}$) were purchased from Sigma-Aldrich and passed through basic alumina before use. 4-Cyano-4-[(dodecylsulfanylthiocarbonyl)sulfanyl]pentanoic acid (CDSPA, 97%), anhydrous *N,N'*-dimethylformamide (DMF) and 2,2'-azobis(2-methylpropionitrile) (AIBN, 98%) were purchased from Sigma-Aldrich and used as received. *Tert*-butyl peroxy-2-ethylhexanoate (Trigonox 21S or T21s) initiator was supplied by AkzoNobel. Deuterated chloroform (CDCl_3) and tetrahydrofuran (TDF) were obtained from Eurisotop. 2-Methylene-4-phenyl-1,3-dioxolane (MPDL), 2-methylene-1,3-dioxepane (MDO) and 5,6-benzo-2-methylene-1,3-dioxepane (BMDO) were prepared from the cyclic bromoacetal intermediate as described elsewhere.^[44] All other solvents were purchased from Carlo-Erba and used as received. [3-(4,5-Dimethylthiazol-2-yl)-2,5-diphenyl tetrazolium bromide] (MTT) was purchased from Sigma-Aldrich and used as received.

2.2. Analytical method

2.2.1. Nuclear magnetic resonance (NMR) spectroscopy. ^1H -NMR spectroscopy was performed in 5 mm diameter tubes in deuterated chloroform (CDCl_3) or tetrahydrofuran (TDF) at 25 °C on a Bruker Avance 300 spectrometer at 300 MHz. The chemical shift

scale was calibrated based on the internal solvent signal (CDCl_3 : $\delta = 7.26$ ppm; TDF: $\delta = 1.72$ and 3.58 ppm).

2.2.2. Size exclusion chromatography (SEC). SEC was performed at $35\text{ }^\circ\text{C}$ with two columns from Polymer Laboratories (PL-gel MIXED-D; 300×7.5 mm; bead diameter, $5\text{ }\mu\text{m}$; linear part, $400\text{--}400\text{ }000\text{ g.mol}^{-1}$) and a differential refractive index detector (Spectrasystem RI-150 from Thermo Electron Corp.). Chloroform was used as eluent at a flow rate of 1 mL.min^{-1} and toluene as a flow-rate marker. A conventional calibration curve was based on poly(methyl methacrylate) (PMMA) standards (peak molar masses, $M_p = 625\text{--}625\text{ }500\text{ g.mol}^{-1}$) from Polymer Laboratories. This technique allowed M_n (number-average molar mass), M_w (weight-average molar mass), and M_w/M_n (dispersity, D) to be determined. SEC of degraded copolymers was performed in the presence of $0.1\text{ vol.}\%$ of trifluoroacetic acid (TFA, 99%) in chloroform (in both the mobile phase and the sample) to avoid the formation of aggregates and/or interaction with the columns because of carboxylic acid chain ends.

2.2.3. Dynamic light scattering (DLS). Nanoparticle diameters, reported in number (D_n), volume (D_v) and intensity (D_z), and particle size distribution (PSD) were measured by dynamic light scattering (DLS) with a Nano ZS from Malvern (173° scattering angle) at a temperature of $25\text{ }^\circ\text{C}$.

2.2.4. Transmission electron microscopy (TEM). Grids were glowing discharged before use. $5\text{ }\mu\text{L}$ of diluted nanoparticle suspensions ($5\text{ }\%$, v/v) were deposited for 30 s on copper grids covered with formvar-carbon film. The excess solution was blotted off using a filter paper. Samples were then stained using uranyl acetate ($2\text{ }\%$, w/v) for $1\text{--}5$

min at room temperature. Then the excess solution was removed using a filter paper. The grids were then analyzed using a JEOL JEM-1400 operating at 80 kV. Images were acquired using an Orius camera (Gatan Inc, USA). The nanoparticles were analyzed by defining the number-average diameter (D_n), the weight-average diameter (D_w), the z-average diameter (D_z) and the polydispersity index (PDI) using the following equations:

$$D_n = \frac{\sum_i n_i \cdot D_i}{\sum_i n_i}$$

$$D_w = \frac{\sum_i n_i \cdot D_i^4}{\sum_i n_i \cdot D_i^3}$$

$$D_z = \frac{\sum_i n_i \cdot D_i^6}{\sum_i n_i \cdot D_i^5}$$

$$\text{PDI} = D_w / D_n$$

2.2.5. Cryogenic transmission electron microscopy (Cryo-TEM). Grids were prepared using a Vitrobot Mark IV (Thermo Fisher), operating at 20 °C and under 100 % humidity. 4 μL of undiluted nanoparticle suspensions were deposited on freshly glow discharged Quantifoil R2/2, 200 mesh grids. The grids were blotted for 5 s with blot force 0, and then plunge-frozen into liquid ethane cooled down at liquid nitrogen temperature. The grids were then analyzed using a Tecnai G20 (FEG, FEI) microscope operating at 200 kV, equipped with a K2 Summit direct-detection camera. Images were recorded at $15.000 \times$ magnification, with a pixel size of 2.5 Å at 20 $\text{e}^-/\text{\AA}^2$.

2.2.6. Optical microscopy. Optical images of cells were captured with an AxioObserver Z1 (Carl Zeiss, Germany) inverted microscope equipped with a XL incubator thermostated at 37°C, a charge-coupled device (CCD) CoolSnap-HQ2 camera (6.45 μm pixel size; Photometrics, Tucson, USA) and an Achroplan 4X/0.10

NA dry objective lens using a brightfield mode (TL halogen lamp). Images (12 bits numerical) were processed using Zen 2.6 software (blue edition).

2.3. Synthetic procedures

2.3.1 Synthesis of poly[oligo(ethylene glycol) methyl ether methacrylate] (POEGMA) macro-chain transfer agent (CTA). The synthesis of POEGMA₂₃ was conducted as follows: in a 50 mL round bottom flask, fitted with a rubber septum and a magnetic stirring bar, a mixture of OEGMA (3.680 g, 0.012 mol), AIBN (9.6 mg, 5.93×10^{-2} mmol), CDSPA (0.097 g, 2.41×10^{-1} mmol, CDSPA/AIBN molar ratio = 4.0) and acetonitrile (25 mL) was degassed by argon bubbling for at least 15 min at room temperature. The mixture was then immersed in a preheated oil bath at 70 °C for 5 h. Monomer conversion was determined by ¹H NMR spectroscopy by integrating the two oxymethylene protons of OEGMA and POEGMA at 4.3 and 4.1 ppm, respectively. After the reaction, the polymer solution was cooled in an ice water bath. Acetonitrile was then removed under reduced pressure and the polymer was precipitated in a large excess of cold 1:1 diethyl ether/petroleum spirit mixture. The purified polymer was dried under high vacuum until constant weight. $DP_{n,NMR}$ was determined by ¹H NMR spectroscopy by integrating the two oxymethylene protons of POEGMA at 4.1 ppm and the eighteen protons of the C₁₂ alkyl chains of CDSPA at 1.2-1.4 ppm. $DP_{n,SEC}$, M_n and D were obtained by SEC.

The same procedure was followed with the following modifications to obtain the POEGMA₅₂ macro-CTA: OEGMA (5.40 g, 0.018 mol), AIBN (4.5 mg, 2.78×10^{-2} mmol), CDSPA (0.050 g, 1.24×10^{-1} mmol) and acetonitrile (12.5 mL).

2.3.2. Block copolymer synthesis. For the sake of clarity, the following abbreviations will now be used: OEGMA = OEG, LMA = L, $m = DP_{n,POEGMA}$, $n = DP_{n,PLMA}$, POEGMA-*b*-PLMA = **OEG_m-L_n** (**MP0** and **MP5**), POEGMA-*b*-P(LMA-*co*-MPDL) = **OEG_m-L_nMP** (**MP1-MP9**), POEGMA-*b*-P(LMA-*co*-BMDO) = **OEG_m-L_nB** (**BM1-BM4**) and POEGMA-*b*-P(LMA-*co*-MDO) = **OEG_m-L_nM** (**M1-M4**).

*Synthesis of poly[oligo(ethylene glycol) methyl ether methacrylate]-*b*-poly[(lauryl methacrylate)-*co*-(2-methylene-4-phenyl-1,3-dioxolane)]* (POEGMA-*b*-P(LMA-*co*-MPDL)). A typical synthesis of POEGMA₂₃-*b*-P(LMA₁₅₀-*co*-MPDL) (**OEG₂₃-L₁₅₀MP**) by RAFT dispersion polymerization at 15 wt.% solids with $f_{MPDL,0} = 0$ (**MP0**) was as follows: in a 40 mL vial, fitted with a rubber septum and a magnetic stirring bar, a mixture of LMA (0.512 g, 2.02×10^{-3} mol), T21s initiator (0.6 mg, 2.78×10^{-3} mmol, dissolved at 0.1% w/v in DMF) and POEGMA₂₃ macro-CTA (0.098 g, 1.32×10^{-2} mmol; macro-CTA/initiator molar ratio = 5.0) in anhydrous DMF (3.41 g, 3.6 mL) was degassed by argon bubbling for at least 15 min and then immersed in a preheated oil bath at 90 °C for 24 h. Samples were periodically withdrawn to determine the LMA conversion by ¹H NMR spectroscopy by integrating the two oxymethylene protons of LMA at 5.5 and 6.0 ppm with PLMA protons at 3.8 ppm. M_n and D were determined by SEC. The nanoparticle colloidal characteristics, D_z and PSD, were obtained by DLS. The nanoparticles were dried under reduced pressure at 40 °C and solubilized in a minimal amount of dichloromethane (DCM) before precipitation in cold methanol. The purified copolymer was collected after centrifugation (10 000 rpm, 30 min) and dried under high vacuum until constant weight.

The same procedure was performed with: $f_{\text{MPDL},0} = 0.2$ (**MP1**) [LMA (0.504 g, 1.99×10^{-3} mol), MPDL (0.081 g, 5.00×10^{-1} mmol), T21s initiator (0.6 mg, 2.78×10^{-3} mmol, dissolved at 0.1% w/v in DMF), POEGMA₂₃ macro-CTA (0.102 g, 1.38×10^{-2} mmol, DMF (3.9 g, 4.1 mL)]; $f_{\text{MPDL},0} = 0.4$ (**MP2**) [LMA (0.511 g, 2.01×10^{-3} mol), MPDL (0.214 g, 1.32×10^{-3} mol), T21s initiator (0.6 mg, 2.78×10^{-3} mmol, dissolved at 0.1% w/v in DMF), POEGMA₂₃ macro-CTA (0.103 g, 1.39×10^{-2} mmol) and DMF (4.7 g, 5.0 mL)]; $f_{\text{MPDL},0} = 0.6$ (**MP3**) [LMA (0.507 g, 2.00×10^{-3} mol), MPDL (0.476 g, 2.94×10^{-3} mol), T21s initiator (0.6 mg, 2.78×10^{-3} mmol, dissolved at 0.1% w/v in DMF), POEGMA₂₃ macro-CTA (0.095 g, 1.28×10^{-2} mmol) and DMF (6.2 g, 6.5 mL)] and $f_{\text{MPDL},0} = 0.7$ (**MP4**) [LMA (0.500 g, 1.97×10^{-3} mol), MPDL (0.785 g, 4.85×10^{-3} mol), T21s initiator (0.6 mg, 2.78×10^{-3} mmol, dissolved at 0.1% w/v in DMF) and POEGMA₂₃ macro-CTA (0.099 g, 1.34×10^{-2} mmol) and DMF (7.6 g, 8.0 mL)].

The same procedure was performed with POEGMA₅₂ macro-CTA, a targeted $DP_{n,\text{PLMA}} = 300$ (**OEG₅₂-L₃₀₀MP**) and with: $f_{\text{MPDL},0} = 0$ (**MP5**) [LMA (0.503 g, 1.98×10^{-3} mol), T21s initiator (0.2 mg, 9.26×10^{-4} mmol, dissolved at 0.1% w/v in DMF) and POEGMA₅₂ macro-CTA (0.107 g, 6.65×10^{-3} mmol) and DMF (3.5 g, 3.7 mL)]; $f_{\text{MPDL},0} = 0.2$ (**MP6**) [LMA (0.500 g, 1.97×10^{-3} mol), MPDL (0.082 g, 5.06×10^{-1} mmol), T21s initiator (0.3 mg, 1.39×10^{-3} mmol, dissolved at 0.1% w/v in DMF) and POEGMA₅₂ macro-CTA (0.105 g, 6.52×10^{-3} mmol) and DMF (3.9 g, 4.1 mL)]; $f_{\text{MPDL},0} = 0.4$ (**MP7**) [LMA (0.503 g, 1.98×10^{-3} mol), MPDL (0.215 g, 1.33×10^{-3} mol), T21s initiator (0.2 mg, 9.26×10^{-4} mmol, dissolved at 0.1% w/v in DMF) and POEGMA₅₂ macro-CTA (0.107 g, 6.65×10^{-3} mmol) and DMF (4.6 g, 4.9 mL)]; $f_{\text{MPDL},0} = 0.6$ (**MP8**)

[LMA (0.510 g, 2.01×10^{-3} mol), MPDL (0.476 g, 2.94×10^{-3} mol), T21s initiator (0.2 mg, 9.26×10^{-4} mmol, dissolved at 0.1% w/v in DMF) and POEGMA₅₂ macro-CTA (0.107 g, 6.65×10^{-3} mmol) and DMF (6.1 g, 6.4 mL)] and $f_{\text{MPDL},0} = 0.7$ (**MP9**) [LMA (0.501 g, 1.97×10^{-3} mol), MPDL (0.758 g, 4.68×10^{-3} mol), T21s initiator (0.2 mg, 9.26×10^{-4} mmol, dissolved at 0.1% w/v in DMF) and POEGMA₅₂ macro-CTA (0.107 g, 6.65×10^{-3} mmol) and DMF (7.6 g, 8.0 mL)].

Synthesis of poly[oligo(ethylene glycol) methyl ether methacrylate]-b-poly[(lauryl methacrylate)-co-(5,6-benzo-2-methylene-1,3-dioxepane)] (POEGMA-*b*-P(LMA-co-BMDO)). A typical synthesis of POEGMA₂₃-*b*-P(LMA₁₅₀-co-BMDO) (**OEG₂₃-L₁₅₀B**) by RAFT dispersion polymerization at 15 wt.% solids and $f_{\text{BMDO},0} = 0.2$ (**BM1**) was as follows: in a 40 mL vial, fitted with a rubber septum and a magnetic stirring bar, a mixture of LMA (0.514 g, 2.02×10^{-3} mol), BMDO (0.080 g, 4.91×10^{-1} mmol), T21s initiator (0.6 mg, 2.78×10^{-3} mmol, dissolved at 0.1% w/v in DMF) and POEGMA₂₃ macro-CTA (0.101 g, 1.37×10^{-2} mmol; macro-CTA/initiator molar ratio = 5.0) in anhydrous DMF (3.8 g, 4.0 mL) was degassed by argon bubbling for at least 15 min and then immersed in a preheated oil bath at 90 °C for 24 h. Determination of LMA conversion and colloidal characteristics of the nanoparticles as well as purification of the copolymers were performed as for **OEG₂₃-L₁₅₀MP**.

The same procedure was performed with: $f_{\text{BMDO},0} = 0.4$ (**BM2**) [LMA (0.501 g, 1.97×10^{-3} mol), BMDO (0.241 g, 1.48×10^{-3} mol), T21s initiator (0.6 mg, 2.78×10^{-3} mmol, dissolved at 0.1% w/v in DMF) and POEGMA₂₃ macro-CTA (0.096 g, 1.30×10^{-2} mmol) and DMF (4.6 g, 4.9 mL)]; $f_{\text{BMDO},0} = 0.6$ (**BM3**) [LMA (0.503 g, 1.98×10^{-3} mol), BMDO (0.241 g, 1.48×10^{-3} mol), T21s initiator (0.6 mg, 2.78×10^{-3} mmol, dissolved at 0.1% w/v in DMF) and POEGMA₂₃ macro-CTA (0.096 g, 1.30×10^{-2} mmol) and DMF (4.6 g, 4.9 mL)].

³ mol), BMDO (0.482 g, 2.96×10^{-3} mol), T21s initiator (0.6 mg, 4.17×10^{-3} mmol, dissolved at 0.1% w/v in DMF) and POEGMA₂₃ macro-CTA (0.099 g, 1.34×10^{-2} mmol) and DMF (6.1 g, 6.4 mL)]; $f_{\text{BMDO},0} = 0.7$ (**BM4**) [LMA (0.504 g, 1.98×10^{-3} mol), BMDO (0.805 g, 4.94×10^{-3} mol), T21s initiator (0.6 mg, 2.78×10^{-3} mmol, dissolved at 0.1% w/v in DMF) and POEGMA₂₃ macro-CTA (0.098 g, 1.32×10^{-2} mmol) and DMF (7.6 g, 8.0 mL)].

Synthesis of poly[oligo(ethylene glycol) methyl ether methacrylate]-b-poly[(lauryl methacrylate)-co-(2-methylene-1,3-dioxepane)] (POEGMA-b-P(LMA-co-MDO)). A typical synthesis of POEGMA₂₃-b-P(LMA₁₅₀-co-MDO) (**OEG₂₃-L₁₅₀M**) by RAFT dispersion polymerization at 15 wt.% solids with $f_{\text{MDO},0} = 0.2$ (**M1**) was as follows: in a 40 mL vial, fitted with a rubber septum and a magnetic stirring bar, a mixture of LMA (0.532 g, 2.09×10^{-3} mol), MDO (0.059 g, 5.18×10^{-1} mol), T21s initiator (0.6 mg, 2.78×10^{-3} mmol, dissolved at 0.1% w/v in DMF) and POEGMA₂₃ macro-CTA (0.095g, 1.28×10^{-2} mmol; macro-CTA/initiator molar ratio = 5.0) in anhydrous DMF (3.7 g, 3.9 mL) was degassed by argon bubbling for at least 15 min and then immersed in a preheated oil bath at 90 °C for 24 h. Determination of LMA conversion and colloidal characteristics of the nanoparticles as well as purification of the copolymers were performed as for **OEG₂₃-L₁₅₀MP**.

The same procedure was performed with $f_{\text{MDO},0} = 0.4$ (**M2**) [LMA (0.520 g, 2.05×10^{-3} mol), MDO (0.150 g, 1.32×10^{-3} mol), T21s initiator (0.6 mg, 2.78×10^{-3} mmol, dissolved at 0.1% w/v in DMF) and POEGMA₂₃ macro-CTA (0.098 g, 1.32×10^{-2} mmol) and DMF (4.3 g, 4.5 mL)], $f_{\text{MDO},0} = 0.6$ (**M3**) [LMA (0.510 g, 2.01×10^{-3} mol),

MDO (0.340 g, 2.98×10^{-3} mol), T21s initiator (0.6 mg, 2.78×10^{-3} mmol, dissolved at 0.1% w/v in DMF) and POEGMA₂₃ macro-CTA (0.095 g, 1.28×10^{-2} mmol) and DMF (5.5 g, 5.8 mL)] and $f_{\text{MDO},0} = 0.7$ (**M4**) [LMA (0.504 g, 1.98×10^{-3} mol), MDO (0.524 g, 4.60×10^{-3} mol), T21s initiator (0.6 mg, 4.17×10^{-3} mmol, dissolved at 0.1% w/v in DMF) and POEGMA₂₃ macro-CTA (0.099 g, 1.34×10^{-2} mmol) and DMF (6.4 g, 6.8 mL)].

2.4. Degradation procedures

2.4.1. Polymer degradation. In a 5 mL vial, 50 mg of purified copolymer was dissolved in 2.5 mL of THF. After solubilization, 2.5 mL of potassium hydroxide solution (KOH, 5 wt.%) in MeOH was added. The cloudy mixture was stirred at room temperature. Samples (1 mL) were periodically withdrawn, immediately dried under vacuum and mixed with 2 mL of chloroform, allowing salts filtration using a 0.2 μm PTFE filter. After filtration, the organic phase was washed three times with HCl (1 mL, 1 mol.L⁻¹). The organic solvent was then removed under reduced pressure and the degradation products were analyzed by SEC with 0.1 vol.% TFA in the eluent.

2.4.2. Nanoparticle degradation. In a 40 mL vial were mixed an aqueous suspension of nanoparticles and an equal volume of aqueous potassium hydroxide (KOH, 5 wt.%). The vial was placed in an orbital shaker (IKA KS4000i control, 37°C, 90 rpm) and samples were withdrawn at different intervals and lyophilized. 2 mL of chloroform was then added to each vial allowing salts filtration by using a 0.2 μm PTFE filter. After filtration, the organic phase was washed three times with HCl (1 mL, 1 mol.L⁻¹). The

organic solvent was then removed under reduced pressure and the degradation products were analyzed by SEC with 0.1 vol.% TFA in the eluent.

2.5. Transfer procedures to water

2.5.1. Dialysis against water. A suspension of nanoparticles was directly poured into a pre-wetted dialysis bag (MWCO 3500, RC membrane) and then dialyzed against water. Water was changed twice a day for three days. The same procedure was also performed except the nanoparticle suspension was diluted 20 times in DMF before dialysis.

2.5.2. Dialysis with an intermediate solvent. A suspension of nanoparticles was directly poured into a pre-wetted dialysis bag (MWCO 3500, RC membrane) and then dialyzed against acetone. Acetone was changed twice a day for three days. After dialysis, the acetone suspension of nanoparticles was transferred to another dialysis bag (MWCO = 3500, RC membrane) and dialyzed against water. Water was changed twice a day for three days.

2.6. Biological evaluation

2.6.1 Cell culture. Human endothelial umbilical vein cells (HUVEC), embryonic murine fibroblast (NIH/3T3) and murine macrophage-monocyte cells (J774.A1) were purchased from American Type Culture Collection (ATCC) and maintained as recommended. Fetal Bovine Serum (FBS) was purchased from Gibco, Penicillin-Streptomycin stabilized solution, Dulbecco's Modified Eagle Medium (DMEM) and Roswell Park Memorial Institute medium (RPMI)-1640 medium were purchased from Sigma-Aldrich and used as received. J774.A1 cells were grown in RPMI-1640

supplemented with 10 % FBS, penicillin (50 U.mL⁻¹) and streptomycin (50 U.mL⁻¹). NIH/3T3 and HUVEC cells were grown in DMEM high glucose supplemented with 10 % FBS, penicillin (50 U.mL⁻¹) and streptomycin (50 U.mL⁻¹). Cells were maintained in a humid atmosphere at 37 °C with 5 % CO₂.

2.6.2 Cell viability assay. In 96-well microtiter plates (TPP, Switzerland), cells were seeded (HUVEC: 2×10^4 cells mL⁻¹, NIH/3T3: 4×10^4 cells mL⁻¹, J774.A1: 2×10^4 cells mL⁻¹) in 100 µL of growth medium and preincubated for 24 h in incubator (37 °C and 5% CO₂). After appropriate dilutions, 100 µL of the copolymer nanoparticles (obtained after intermediate dialysis in acetone to remove remaining monomer, see part 3.3) in cell culture medium (0.01, 0.05, 0.1 and 0.5 mg.mL⁻¹) was added over the cells and incubated for 72 h. A MTT solution (5 mg.mL⁻¹) was prepared with phosphate buffered saline (PBS) and filtered with sterile filters (0.2 µm). At the end of incubation period, 20 µL of MTT solution was added to each well. After incubation (1 h for HUVEC and J774.A1 cells, 1.5 h for NIH/3T3 cells), the medium was removed and 200 µL of dimethylsulfoxide (DMSO) was then added to each well to dissolve the formazan crystals. The absorbance was then measured by a microplate reader (LAB Systems Original Multiscan MS) at 570 nm. Cell viability was calculated as the absorbance ratio between treated and untreated control cells. All experiments were performed in triplicate to determine means and SD.

3. Results and Discussion

3.1 Design rationale

Previous work in rROPISA was limited to the synthesis of non-aqueous suspensions of CKA-containing poly(lauryl methacrylate)-*b*-poly(benzyl methacrylate) (PLMA-*b*-PBzMA) nanoparticles in heptane to prevent early hydrolysis of CKA monomers/repeat units.^[38,45] Their hydrophobic PLMA stabilizing shell therefore prevents any subsequent transfer to aqueous media. In this context, we designed a simple two-step rROPISA system allowing for the synthesis of stable aqueous suspensions of degradable particles by first performing rROPISA in DMF as a water-miscible polar solvent, followed by transfer of the particles to water during which their colloidal properties were preserved.

The idea was to choose poly[oligo(ethylene glycol) methyl ether methacrylate] (POEGMA) as the solvophilic block given its solubility in both water and many polar organic solvents including DMF (Figure 2). Also, POEGMA is a well-known PEG-based polymer used in the biomedical field, owing to its biocompatibility and to the stealth properties it confers to nanoparticles or therapeutics.^[39–43,46–48] PLMA was selected as a solvophobic block according to its non-solubility in DMF and the ability of LMA to copolymerize with CKAs such as MPDL and BMDO.^[38] These two aromatic ring-containing CKAs were first tested before investigating the use of MDO, which has the same structure as polycaprolactone, a well-known polymer approved for use in humans.^[49]

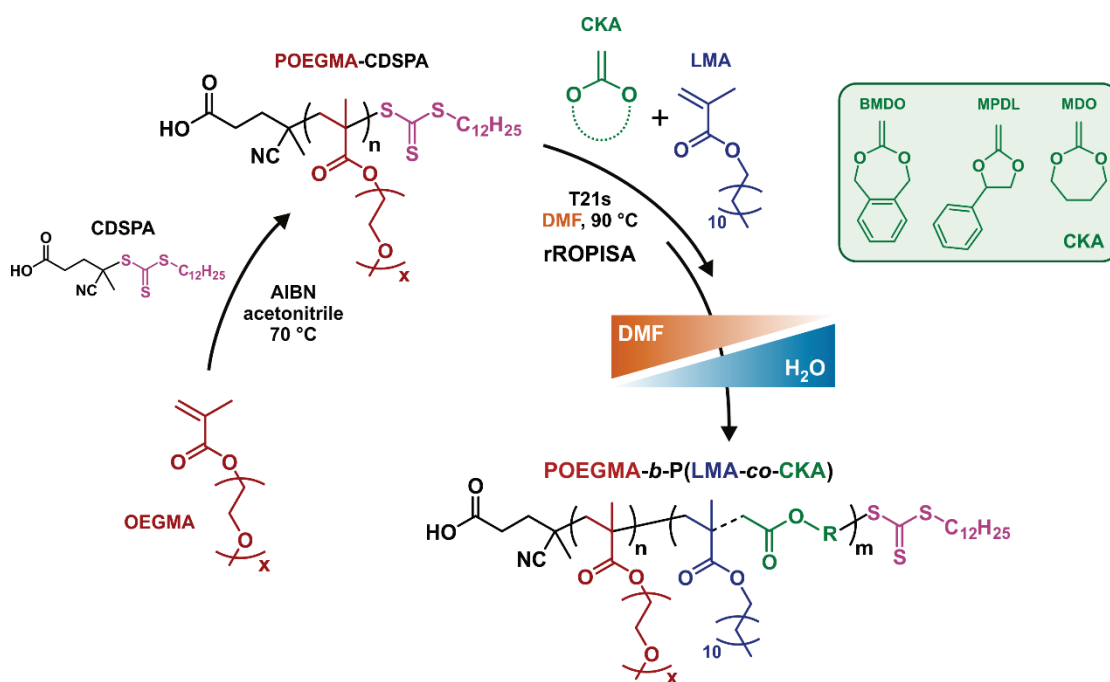


Figure 2. RAFT-mediated synthesis of poly[oligo(ethylene glycol) methyl ether methacrylate] (POEGMA) chain transfer agent followed by radical ring-opening copolymerization-induced self-assembly (rROPISA) in DMF at 90°C of lauryl methacrylate (LMA) and cyclic ketene acetals (CKAs), followed by transfer to water to produce aqueous suspensions of POEGMA-*b*-P(LMA-co-CKA) (OEG_m-L_nCKA) diblock copolymer nanoparticles.

3.2 Application to the three main CKAs

3.2.1 Application to MPDL. Well-defined POEGMA₂₃ ($M_{n,SEC} = 7\,400\text{ g}\cdot\text{mol}^{-1}$, $\bar{D} = 1.09$) and POEGMA₅₂ ($M_{n,SEC} = 16\,100\text{ g}\cdot\text{mol}^{-1}$, $\bar{D} = 1.15$) macro-CTAs were first synthesized by RAFT solution polymerization of OEGMA in acetonitrile at 70 °C for 5 h using CDSPA as a CTA and AIBN as a radical initiator (Table S1, Figure S1).

The POEGMA₂₃ macro-CTA was then chain-extended by copolymerization of LMA (targeted $DP_{n,PLMA} = 150$) with variable initial amounts of MPDL ($f_{MPDL,0} = 0$ –0.7) at 15 wt.% solids in DMF at 90 °C in the presence of T21s as a radical initiator (OEG₂₃-L₁₅₀MP, MP0-MP4, Figure 2). After 24 h, high monomer conversions (~80–90 %) were obtained except with MP4 ($f_{MPDL,0} = 0.7$), for which the polymerization

kinetics was slower (Table S2 and Figure 3a). Linear evolutions of M_n values with conversion and reasonably low dispersities ($\mathcal{D} = 1.2\text{--}1.4$ below 50% conversion) were obtained for all copolymerizations (Figure 3b), with no noticeable impact of the presence of MPDL when compared to **MP0** ($f_{\text{MPDL},0} = 0$).

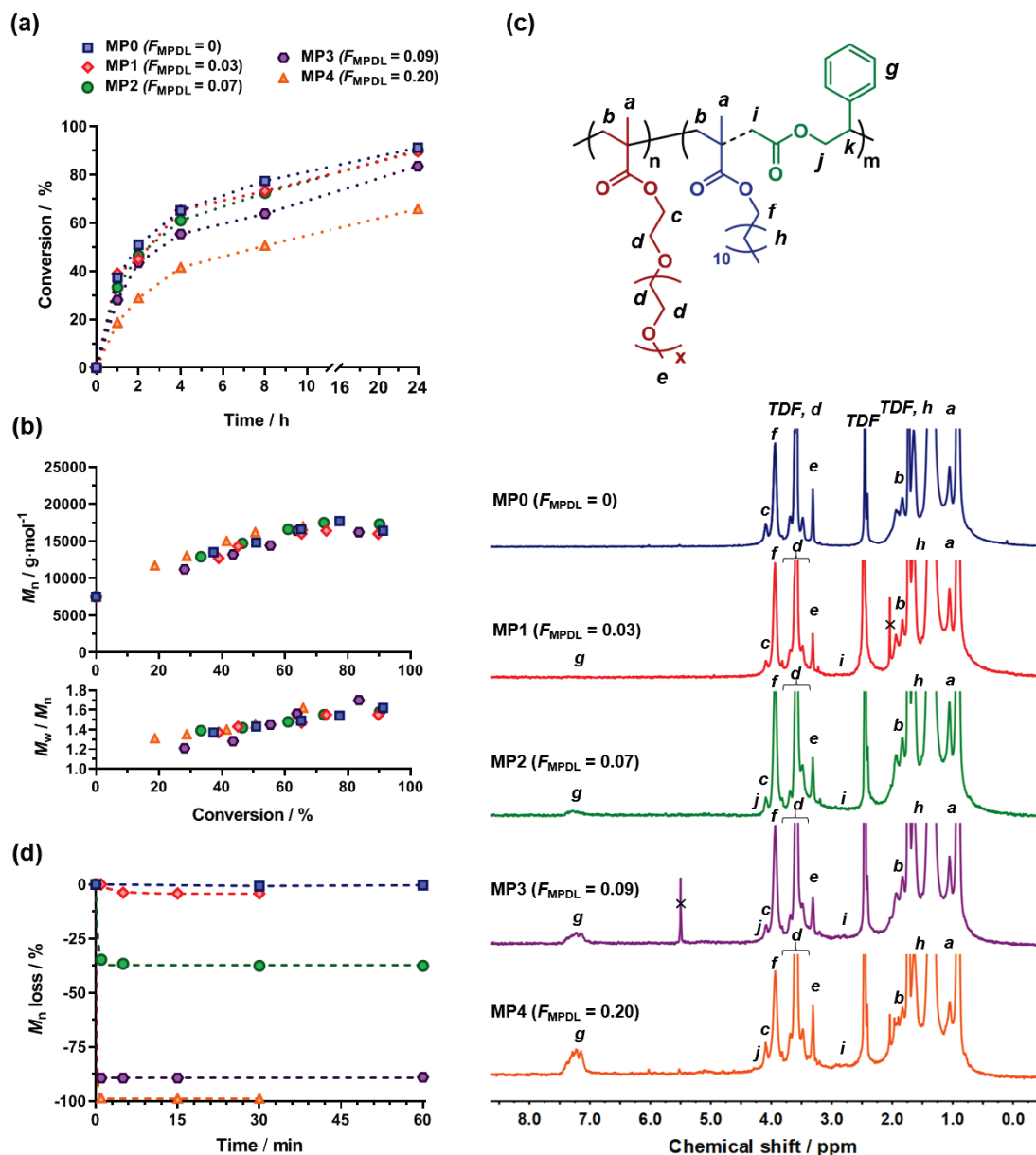


Figure 3. Synthesis of **OEG₂₃-L₁₅₀MP** copolymer nanoparticles (**MP0-MP4**) by RAFT-mediated dispersion copolymerization of LMA and MPDL from a POEGMA₂₃ macro-CTA in DMF at 90 °C as function of $f_{\text{MPDL},0}$: (a) LMA conversion vs. time (dashed lines connecting data points are guides for the eye only); (b) M_n and dispersity (M_w/M_n) of the copolymers vs. LMA conversion determined by SEC; (c) ¹H NMR spectra in TDF of the copolymers in the 0–8.5 ppm region and (d) evolution with time of their M_n loss during degradation under accelerated conditions (dashed lines represent the exponential one phase decay fits).

The structure of POEGMA-*b*-P(LMA-*co*-MPDL) copolymers was confirmed by ¹H NMR spectroscopy (Figure 3c), with in particular, the successful insertion of MPDL as

shown by the aromatic protons *g*. Their integration increased with $f_{\text{MPDL},0}$ and gave molar fractions in the copolymer, F_{MPDL} , ranging from 0 to 0.20 (Table S2). The presence of ester groups in the copolymer was confirmed by hydrolytic degradation under accelerated conditions (THF/MeOH, KOH 2.5 wt.%). While **MP0** ($f_{\text{MPDL},0} = 0$) let the M_n unchanged, **MP1-MP4** ($f_{\text{MPDL},0} = 0.2\text{--}0.7$) copolymers gave a decrease in M_n (Figure 3d), as shown by the shifts of the SEC chromatograms towards lower M_n values (Figure S2). As expected, the higher F_{MPDL} (or $f_{\text{MPDL},0}$), the lower the final M_n after degradation, that reached 25 000, 13 100, 2 700 and 200 g.mol⁻¹ for $F_{\text{MPDL}} = 0.03, 0.07, 0.09$ and 0.20, respectively (Table S3). Those values are in the same order of magnitude than the theoretical ones for the highest amounts of MPDL (Table S3). The discrepancy at low MPDL contents may be explained by the non-negligible amount of closed MPDL units in the copolymer, as already seen with this CKA.^[50]

The onset of the micellar nucleation and the formation of particles occurred after 0.5-1 h, as evidenced by the change in appearance of the polymerization medium from transparent to opalescent. After the polymerizations, stable suspensions of POEGMA-*b*-P(LMA-*co*-MPDL) nanoparticles in DMF were obtained exhibiting average intensity-diameters (D_z) in the 72–109 nm range and particle size distributions (PSD) all below 0.1, indicating narrowly dispersed nanoparticles (Table S2).

The **OEG₂₃-L₁₅₀MP** nanoparticles were then transferred to water through a simple dialysis step. Direct dialysis against water gave stable nanoparticle suspensions only for $F_{\text{MPDL}} \leq 0.07$, likely because of the strong hydrophobicity of unreacted MPDL that altered the colloidal stability. However, when all nanoparticles were diluted 1:20 with

DMF prior dialysis, highly stable nanoparticles with narrow PSD (0.01–0.03) were obtained for all F_{MPDL} values (Table S2, Figure 4 and S3). Importantly, their average diameters were preserved after dialysis, with however a noticeable increase in the nanoparticles' size for high MPDL contents (Figure 4a–e). TEM experiments revealed the formation of nanoparticles with spherical morphology (Figure 4f–o). Their average diameters and size distributions were in good agreement with DLS data except for the copolymer with the highest amount of MPDL whose PSD was already broad according to DLS, presumably due to the presence of micro-particle aggregates during TEM sample preparation.

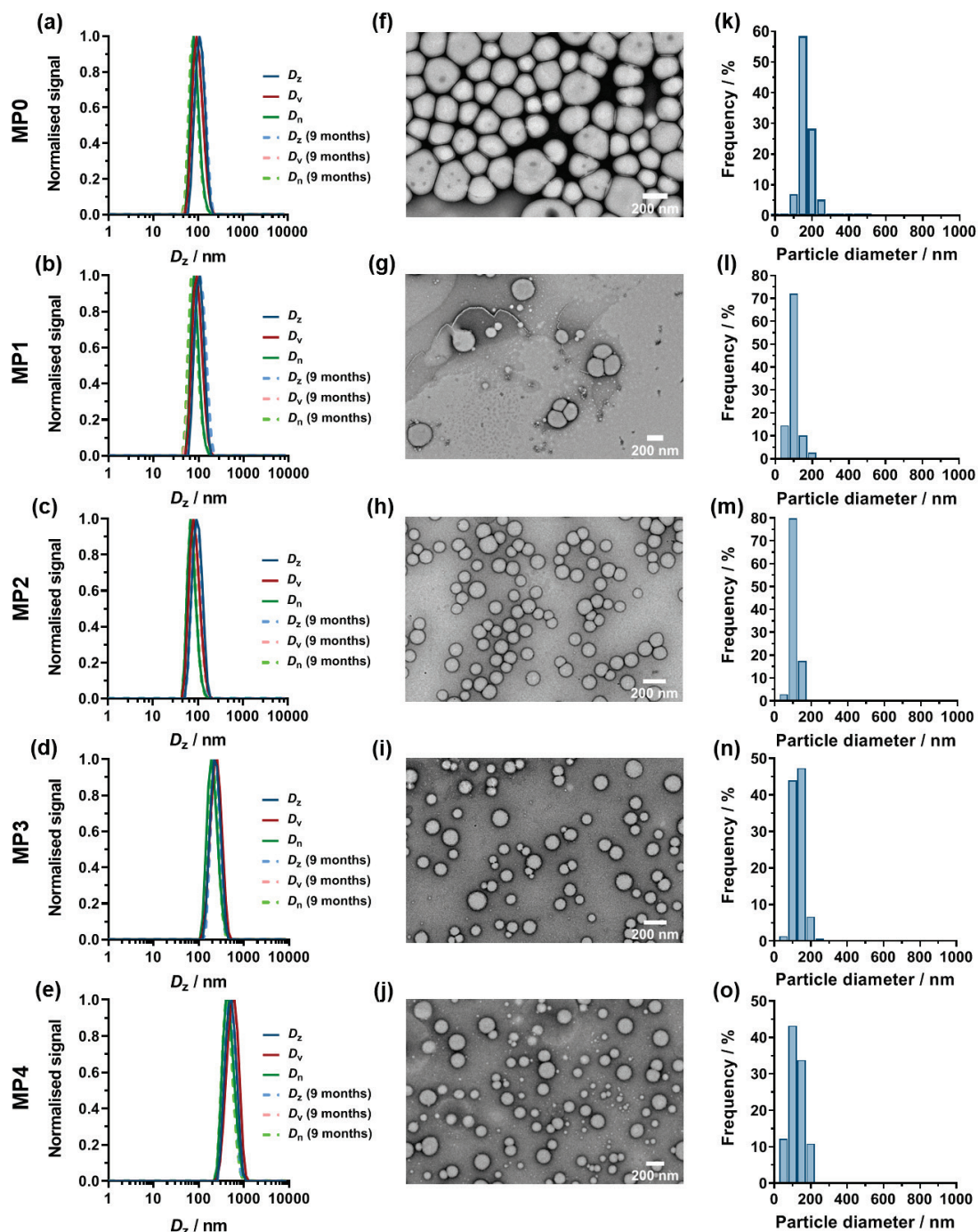


Figure 4. Colloidal characteristics of **OEG₂₃-L₁₅₀MP** nanoparticles **MP0–MP4** after a 1:20 dilution in DMF and dialysis against water: (a–e) average diameters from DLS reported in number (D_n), volume (D_v) and intensity (D_z) distribution after formulation and after 9 months; (f–j) representative TEM images and (k–o) particle size distributions ($n = 75\text{--}800$). TEM data (D_n , D_w , D_z , and PDI) are in Table S4.

All nanoparticles also exhibited very high colloidal stability with no or little variation of their average diameters or their dispersity ($PSD = 0.01\text{--}0.03$) after at least 9 months (Figure 4a–e), which demonstrated the robustness of the 2-step rROPISA process for the preparation of stable aqueous suspensions of CKA-containing nanoparticles.

Similar rROPISA experiments were then performed with the longest macro-CTA (POEGMA₅₂) to potentially improve the preservation of the nanoparticles' colloidal properties at high MPDL contents upon their transfer to water, as suggested by its superior stabilization properties during rROPISA in heptane.^[51] Copolymerizations of LMA (targeted $DP_{n,PLMA} = 300$) and MPDL ($f_{MPDL,0} = 0\text{--}0.7$) were performed in DMF under the same experimental conditions as previously described in order to produce **OEG₅₂-L₃₀₀MP** copolymer nanoparticles (**MP5–MP9**, Table S2). Very similar results in terms of conversions (70–88%) and control of the polymerizations ($M_n = 37.0\text{--}22.9$ kg.mol⁻¹, $D = 1.54\text{--}1.86$) were obtained, with however an overall increase in size of the nanoparticles ($D_z = 113\text{--}168$ nm, $PSD = 0.10\text{--}0.22$). Interestingly, the MPDL contents were also mostly higher (Table S2, Figure S4a), resulting in more pronounced hydrolytic degradation under accelerated conditions for **OEG₅₂-L₃₀₀MP** copolymers than the **OEG₂₃-L₁₅₀MP** counterparts for the same $f_{MPDL,0}$ value (Figure S2 and S4b). It also resulted in a slightly better agreement between predicted and experimental M_n values after degradation (Table S5).

Dialysis of **OEG₅₂-L₃₀₀MP** nanoparticles against water also led to stable aqueous suspensions of spherical nanoparticles with narrow PSD as shown by DLS and TEM (Table S2 and S4, Figure S3 and S5). Interestingly, conversely to **OEG₂₃-L₁₅₀MP**

nanoparticles, they exhibited a much better preservation of their colloidal characteristics even for nanoparticles with the highest MPDL contents (Table S2 and Figure 5), together with a better agreement between average diameters determined by DLS and TEM.

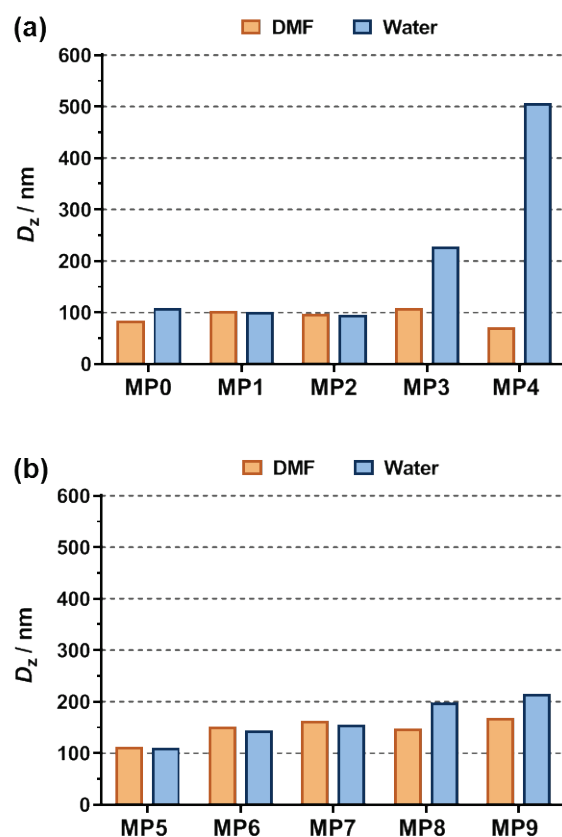


Figure 5. Intensity-average diameters (D_z) of: (a) **OEG₂₃-L₁₅₀MP (MP0-MP4)** and (b) **OEG₅₂-L₃₀₀MP (MP5-MP9)** nanoparticles in DMF (orange bars) and after a 1:20 dilution in DMF followed by dialysis against water (blue bars).

3.2.2 Application to BMDO. The 2-step rROPISA process was then successfully applied to BMDO, which is still one of the most popular CKAs used in rROP. **OEG₂₃-L₁₅₀B** copolymers nanoparticles were obtained by chain-extension of POEGMA₂₃ macro-CTA by copolymerization of LMA and BMDO ($f_{\text{BMDO},0} = 0.2\text{--}0.7$) under the

same experimental conditions as for **OEG₂₃-L₁₅₀MP** copolymers (Figure S6 and Table S6). In general, very similar results were obtained compared to MPDL. However, a better control of the polymerizations was achieved ($\bar{D} = 1.23\text{--}1.50$), together with a slight increase in the BMDO content in the obtained copolymers (Table S6).

Degradation of **OEG₂₃-L₁₅₀B** copolymers under accelerated conditions confirmed their tunable degradability as function of $f_{\text{BMDO},0}$ (Table S7, Figure S6b and S7a–d). The degradation was very similar to that of **OEG₂₃-L₁₅₀MP** copolymers with nonetheless a much more pronounced decrease in M_n when $f_{\text{BMDO},0} = 0.4$ (-75% vs. -38%) owing to its higher BMDO content ($F_{\text{BMDO}} = 0.15$ vs. $F_{\text{MPDL}} = 0.07$).

Narrowly dispersed nanoparticles were also obtained ($\text{PSD} \leq 0.06$), but with smaller diameters ($D_z = 53\text{--}78$ nm) than MPDL-containing nanoparticles (Table S6). After diluted dialysis against water, very stable nanoparticles were obtained and with average diameters in the range 93–161 nm and excellent retention of their narrow PSD (Figure 6 and S3). Interestingly, no significant size increase was obtained for **OEG₂₃-L₁₅₀B** nanoparticles with the highest amounts of BMDO, as they all remained below 200 nm in diameter (Figure S8a). The colloidal properties obtained by TEM were in good agreement with DLS measurements and also showed spherical morphologies (Figure 6).

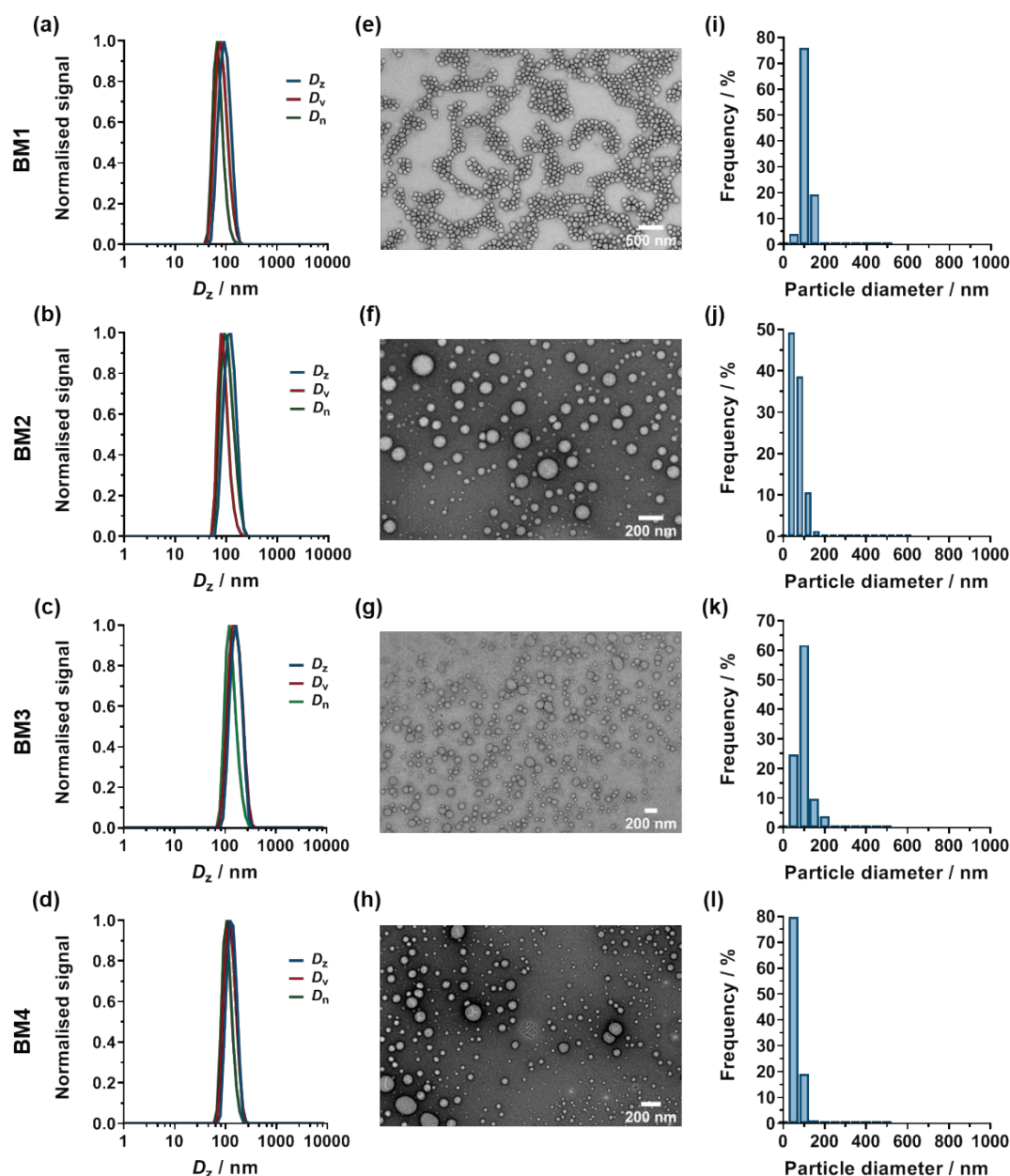


Figure 6. Colloidal characteristics of **OEG₂₃-L₁₅₀B** nanoparticles **BM1–BM4** after a 1:20 dilution in DMF and dialysis against water: (a–d) average diameters from DLS reported in number (D_n), volume (D_v) and intensity (D_z) distribution after formulation; (e–h) representative TEM images and (i–l) particle size distributions ($n = 150$ – 1200). TEM data (D_n , D_w , D_z , and PDI) are in Table S8.

3.2.3 Application to MDO. Even if rROPISA in heptane with MDO as a CKA was successful, it gave high dispersities up to 4 and thus a partial loss of control.^[38] Herein, rROPISA in DMF under similar conditions achieved a much better control of the

copolymerization (Table S9) with $M_n = 14.1\text{--}19.2 \text{ kg.mol}^{-1}$ and $D = 1.57\text{--}1.80$. ^1H NMR spectroscopy attested that **OEG₂₃-L₁₅₀M** copolymers were synthesized (Figure S9a) with $F_{\text{MDO}} = 0.08\text{--}0.15$, depending on the initial comonomer feed.

All copolymers exhibited nearly complete degradation under accelerated conditions (Figure S9b) and excellent agreement with the predicted values (Table S10, Figure S7e–h), suggesting a very high proportion of open MDO. The same transfer procedure to water resulted in stable nanoparticles with spherical morphologies and narrow PSD as observed by DLS and TEM, except for $f_{\text{MDO},0} = 0.7$ (**M4**) that also gave a fraction of microparticles (Figure 7). Not only was there no significant variation in their average diameters after dialysis against water ($D_z = 131\text{--}170 \text{ nm}$), but they were also fairly constant regardless of copolymer composition (Figure S3, S8b, Table S9).

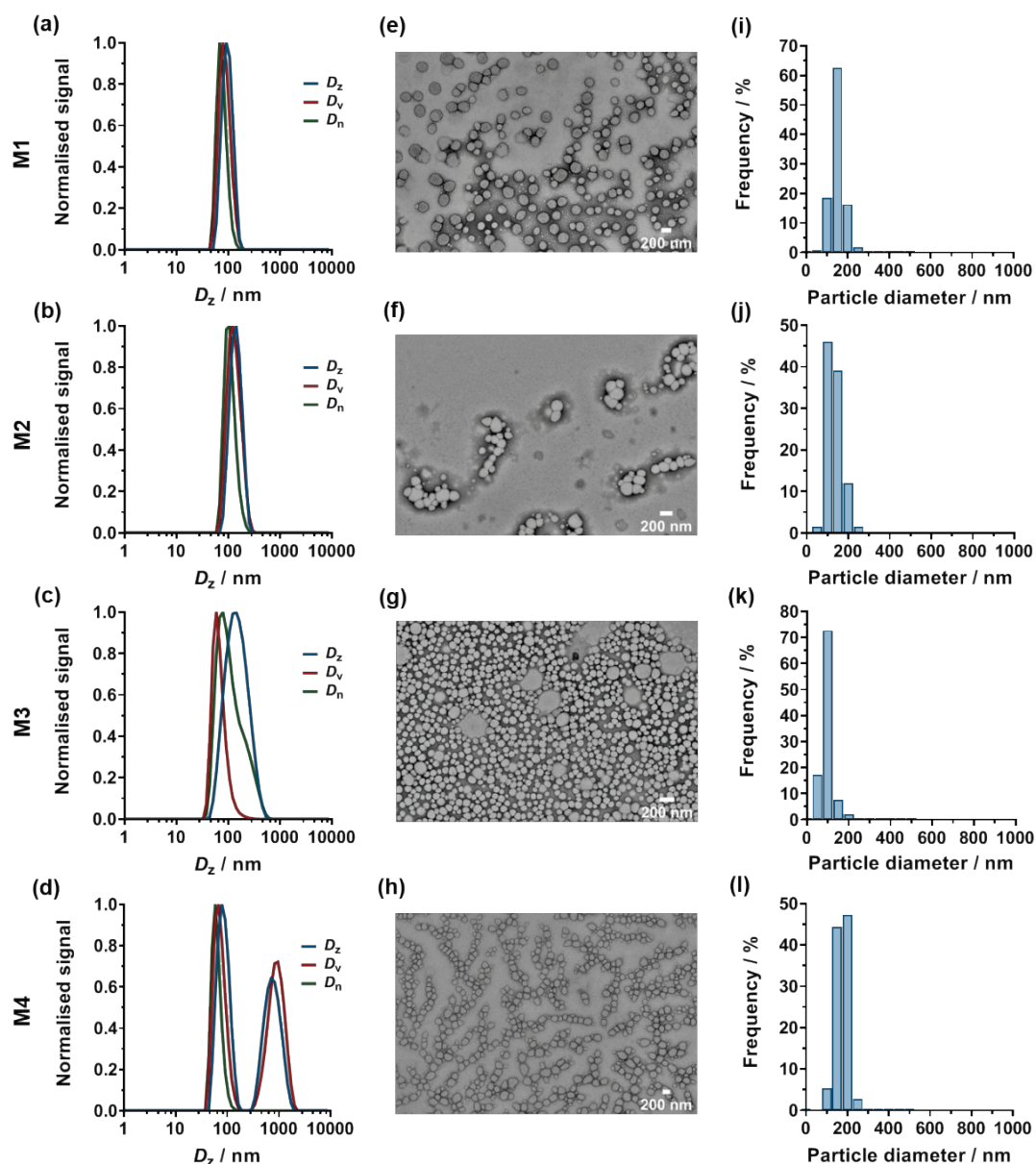


Figure 7. Colloidal characteristics of **OEG₂₃-L₁₅₀M** nanoparticles **M1–M4** after a 1:20 dilution in DMF and dialysis against water: (a–d) average diameters from DLS reported in number (D_n), volume (D_v) and intensity (D_z) distribution after formulation; (e–h) Representative TEM images and (i–l) particle size distributions ($n = 200$ – 500). TEM data (D_n , D_w , D_z , and PDI) are in Table S11.

Importantly, **OEG₂₃-L₁₅₀M** nanoparticles in DMF could also be directly dialysed against water, thus maintaining their original concentrations as opposed to **OEG₂₃-L₁₅₀MP** and **OEG₂₃-L₁₅₀B** nanoparticles that required a preliminary 1:20 dilution in

DMF (Figure S10 and S11). **OEG₂₃-L₁₅₀M** nanoparticles exhibited colloidal stability as high as the other nanoparticles, well-preserved average diameters and narrow PSD ($D_z = 113\text{--}154$ nm, PSD = 0.03–0.14) up to $F_{\text{MDO}} = 0.13$ (Table S12).

3.3 Optimization of the transfer to water

The rROPISA process was then further optimized to allow all types of CKA-containing nanoparticles to be obtained in water without preliminary dilution, thus maximizing their aqueous concentrations. As previously hypothesized, we suspected that, for high $f_{\text{CKA},0}$ values, unreacted MPDL/BMDO caused colloidal instability of **OEG₂₃-L₁₅₀MP** and **OEG₂₃-L₁₅₀B** nanoparticles during their dialysis against water. This limitation was resolved by performing an intermediate dialysis against acetone. Not only the unreacted monomer was efficiently removed, as shown by ¹H-NMR (Figure S12), but it also enabled the resultant nanoparticles to be successfully transferred to water by dialysis without dilution, even for the highest $f_{\text{CKA},0}$ values (Figure S13). DLS measurements mostly showed little variation in diameters when passing from acetone to water and confirmed the excellent colloidal characteristics of **OEG₂₃-L₁₅₀MP** and **OEG₂₃-L₁₅₀B** nanoparticles in water in terms of size and particle size distribution (Figure 8 and Table S13). Average diameter in acetone was ~140 nm (PSD ~0.08) while in water it reached ~120 nm (PSD ~0.11). This procedure was also successfully applied to **OEG₅₂-L₃₀₀MP** and **OEG₂₃-L₁₅₀M** nanoparticles to show the versatility of the process. These two additional series of nanoparticles exhibited great colloidal stability with good

preservation of their average diameters, despite slight broadening of the PSD for the highest CKA contents (Table S13).

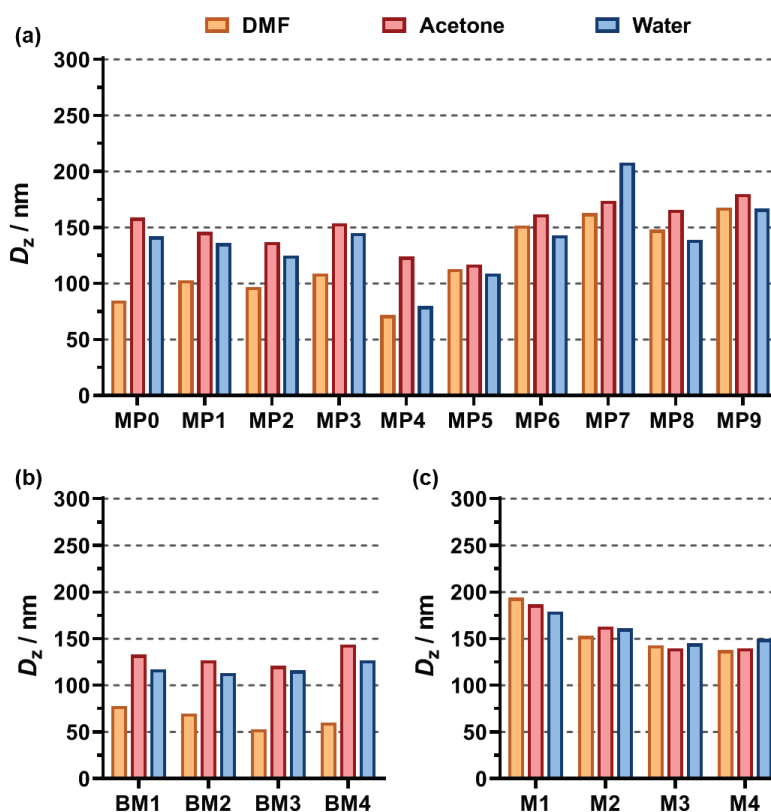


Figure 8. Intensity-average diameters of: (a) OEG_{23} - L_{150} MP (MP0-MP4) and OEG_{52} - L_{300} MP (MP5-MP9); (b) OEG_{23} - L_{150} B (BM1-BM4) and (c) OEG_{23} - L_{150} M (M1-M4) nanoparticles in DMF (orange bars), after direct dialysis against acetone (red bars) and followed by dialysis against water (blue bars).

Interestingly, cryo-TEM was used as a complementary technique to TEM and confirmed the spherical morphology for OEG_{23} - L_{150} MP and OEG_{52} - L_{300} MP nanoparticles (Figure S14), in good agreement with DLS data (Table S13) and TEM observations of their counterparts obtained without intermediate dialysis in acetone (Table S2).

3.4 Degradation of the nanoparticles

After having shown the tunable hydrolytic degradation of the copolymers under accelerated conditions, degradation of the nanoparticles in aqueous suspension was investigated in 2.5 wt.% KOH at 37 °C. Nanoparticles responded quickly to hydrolysis (< 24 h) and exhibited tunable degradation as function of F_{CKA} with decrease in M_n up to > 95% (Figure S15 and 9). Overall, the degradation kinetics and the final M_{ns} after degradation of the different copolymer nanoparticles were similar to those of the corresponding free copolymers.

These results suggested that, regardless of the CKA used, important water uptake by the nanoparticles successfully occurred, resulting in significant degradation. It is also worth noting that this is the first time that extensive hydrolytic degradation of CKA-containing nanoparticles synthesized by polymerization in dispersed medium is reported.

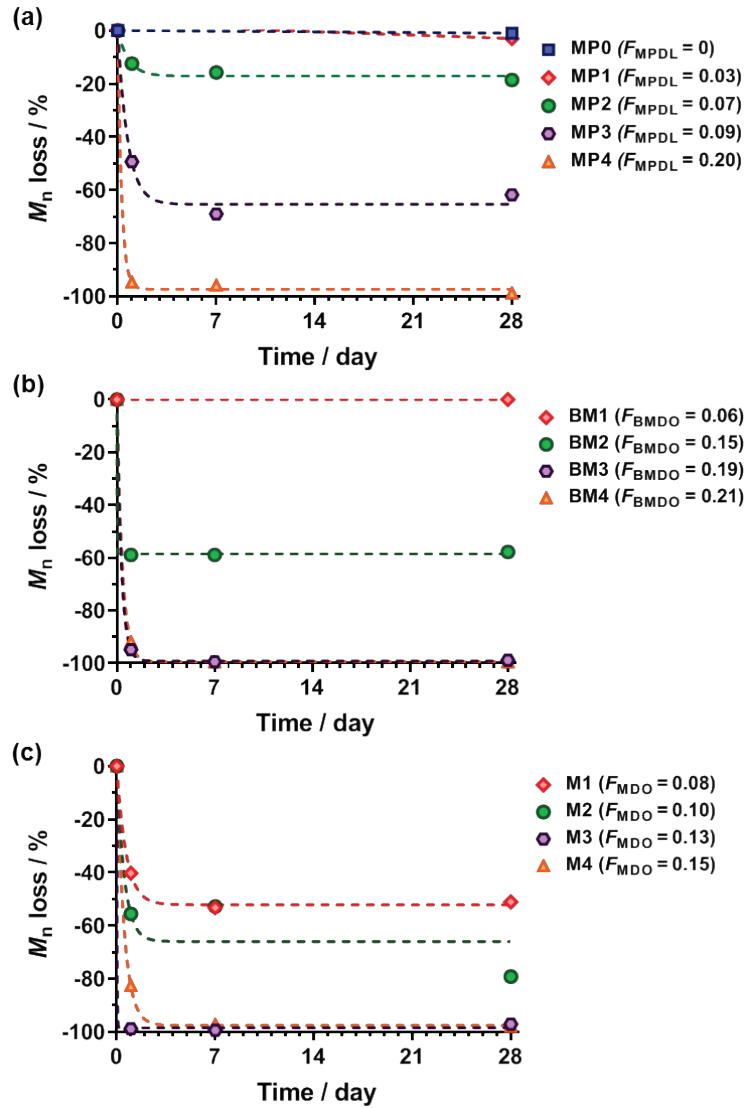


Figure 9. Evolution with time of the number-average molar mass (M_n) loss during degradation under accelerated conditions (2.5% KOH in water) of **OEG₂₃-L₁₅₀CKA** copolymer nanoparticles with the molar fraction of CKA (F_{CKA}) in the copolymer: (a) **OEG₂₃-L₁₅₀MP (MP0-MP4)** copolymers nanoparticles ($F_{MPDL} = 0-0.20$); (b) **OEG₂₃-L₁₅₀BM (BM1-BM4)** copolymers nanoparticles ($F_{BMDO} = 0.06-0.21$) and (c) **OEG₂₃-L₁₅₀M (M1-M4)** copolymers nanoparticles ($F_{MDO} = 0.08-0.15$). Dashed lines represent the exponential one phase decay fit.

3.5 Cytocompatibility

To show the broad applicability of these degradable vinyl copolymer nanoparticles, and for instance to consider their use for biomedical applications, their cytocompatibility was tested on three representative healthy cell lines via both cell viability assays and

cell morphology observations. The cell lines used were: (i) murine macrophages (J774.A1), which are monocyte cells that play a key role in phagocytosis; (ii) human umbilical vein endothelial cells (HUVEC), which are widely used primary endothelial cells for in vitro studies of the vasculature and (iii) murine fibroblasts (NIH/3T3), which are one of the most commonly used fibroblast cell lines. Although there have been examples of cytocompatible CKA-containing copolymers and copolymers formulated into nanoparticles,^[8,45,52,53] the cytocompatibility of CKA-containing nanoparticles obtained by polymerization in dispersed media towards healthy cells has never been investigated.

Three representative libraries of nanoparticles were selected: (i) **OEG₂₃-L₁₅₀MP** and **OEG₂₃-L₁₅₀M**, to investigate potential influence of the nature of the CKA and (ii) **OEG₅₂-L₃₀₀MP**, to evaluate the effect of the POEGMA block length. For each series of nanoparticles, the CKA content was varied ($f_{\text{CKA},0} = 0\text{--}0.7$) to probe its effect on the cell viability. Note that **OEG₂₃-L₁₅₀B** nanoparticles were not tested due to their structural similarity to **OEG₂₃-L₁₅₀MP** nanoparticles. Overall, all types of nanoparticles exhibited cell viability in the 70–100% range up to 0.1 mg.mL⁻¹ for NIH/3T3 cells and up to 0.5 mg.mL⁻¹ for J774.A1 and HUVEC cells (Figure 10a-c). It should be noted that these relatively high concentrations do not reflect their expected use but would rather overexpress any cytotoxic effects arising from the copolymer structures or from their degradation products. Interestingly, despite their sensitivity to foreign materials due to their phagocytic functions resulting in engulfment of

nanoparticles, macrophages (J774.A1 cells) exhibited cell viability greater than 80% for all nanoparticle concentrations.

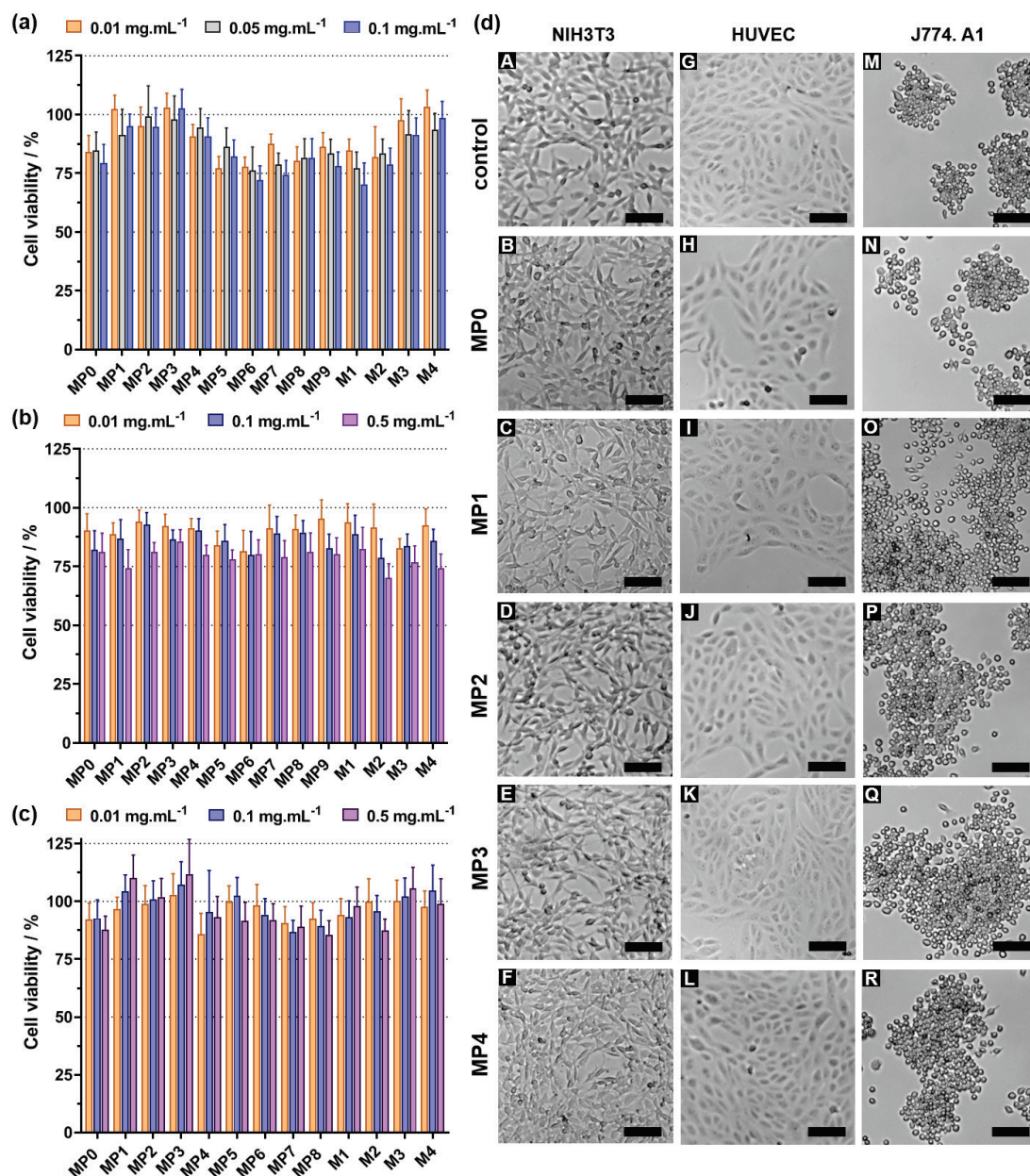


Figure 10. Cell viability (MTT assay) after incubation of: (a) NIH/3T3 cells; (b) HUVEC cells and (c) J774.A1 cells with **OEG_m-L_nMP** ($f_{MPDL,0} = 0-0.7$, **MP0-MP9**) and **OEG₂₃-L₁₅₀M** ($f_{MDO,0} = 0.2-0.7$, **M1-M4**) nanoparticles at different concentrations. Results were expressed as percentage of absorption of treated cells \pm SD in comparison with untreated cells (control). (d) Representative optical images of NIH/3T3 (A-F), HUVEC (G-L), and J774.A1 cells (M-R) after incubation for 72 h with **MP0-MP4** nanoparticles at 0.1 mg.mL⁻¹. Scale bar = 100 μm.

Looking at each set of results individually, it appeared that increasing the nanoparticle concentration over this range had no significant influence on the viability of J774.A1 and NIH/3T3 cells, and only little influence on that of HUVEC cells (especially for **OEG₂₃-L₁₅₀M** nanoparticles), which seems to corroborate previous cytocompatibility studies on CKA-containing water-soluble copolymers.^[52] Increasing the amount of CKA however seemed to conduct to higher cell viabilities of NIH/3T3 cells especially for **OEG₂₃-L₁₅₀MP** and **OEG₂₃-L₁₅₀M** nanoparticles. No significant effect was observed on the three cell lines when increasing the POEGMA chain length with **OEG₅₂-L₃₀₀MP** nanoparticles.

An observation of cell morphology was performed after a 72-hour incubation period of the three cell lines with the nanoparticles at the same concentrations as a complementary method to the cell viability assays to assess their cytocompatibility (Figure 10d and Figure S16-23). Overall, cells treated with the nanoparticles, whatever their nature, exhibited no noticeable difference in terms of morphology (e.g., round-like shape for J774.A1 cells, cobblestone-like morphology for HUVEC cells and fibroblast-like shape for NIH/3T3 cells), size, density or cell proliferation compared to untreated cells, thus confirming the results from the cell viability assays. Therefore, there was no adverse effect of nanoparticles at these concentrations, regardless of the nature of the CKA, its content and the POEGMA chain length. In conclusion, all these results attested for their cytocompatibility and are promising for their ultimate biocompatibility.

4. Conclusion

In this study, we reported on a simple two-step rROPISA process that allowed to readily produce stable, aqueous suspensions of mostly narrowly dispersed, degradable vinyl copolymer nanoparticles. It relied on RAFT-mediated copolymerization of LMA and CKA in DMF at 15 wt.% solid contents from a solvophilic POEGMA macro-CTA. The resulting nanoparticles were then transferred to water by simple dialysis during which their colloidal properties were maintained.

Several key structural parameters were varied such as the nature of the CKA, its content in the copolymer and the POEGMA macro-CTA chain length. It was shown that this two-step rROPISA process was perfectly applicable to the three main CKAs use in rROP (i.e., MPDL, BMDO and MDO) and led to tunable CKA contents up to 21 mol.%, thus demonstrating its versatility and robustness. Increasing the POEGMA chain length helped to improve the colloidal properties upon transfer to water especially for high CKA contents. While MDO-containing nanoparticles could be directly transferred to water, the two-step rROPISA process was further optimized for MPDL- and BMDO-containing copolymers by adding an intermediate dialysis in acetone. It allowed both high concentrations of narrowly dispersed nanoparticles in water to be obtained in the 80–250 nm range and removal of unreacted monomer.

Degradation experiments showed that both free copolymers and corresponding nanoparticles were degradable under accelerated conditions depending on their CKA content. Cytotoxicity studies performed on several libraries of nanoparticles via cell viability assays and cell morphology observations, showed no cytotoxicity up to 0.1 or

0.5 mg.mL⁻¹ on three representative healthy cell lines. With their PEG-based shell, which is known to confer stealth properties, these results make it possible to envisage the use of these nanoparticles in the biomedical field.

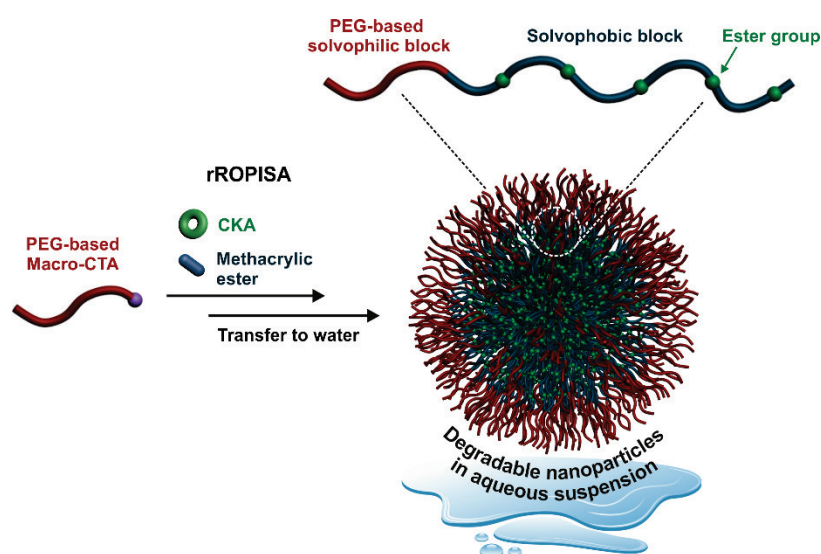
Given its benefits, we believe such a polymerization process to be a promising tool to generate degradable vinyl polymer nanoparticles with great potential for drug delivery applications. Importantly, such approach could also be beneficial to other research fields as degradable particles could favorably replace traditional latexes to yield more environmentally friendly materials. In this context, this two-step rROPISA process could be an important step forward against plastic pollution which has become one of the most pressing environmental problems.

Acknowledgement

We thank the China Scholarship Council (CSC) for the PhD fellowship (2017-2021) of CZ. The authors thank Claire Boulogne and Cynthia Gillet (I2BC, Gif-sur-Yvette, France) for technical assistance in TEM, Ana-Andreea Arteni and Malika Ouldali (I2BC, UMR 9198 Institut de Biologie Intégrative de la Cellule, Gif-sur-Yvette, France) for technical assistance in Cyro-TEM and Valerie Nicolas (MIPSIT, Châtenay-Malabry, France) for the technical assistance in optical microscopy. The CNRS is also acknowledged for financial support.

Table of Content

A simple two-step radical ring-opening copolymerization-induced self-assembly (rROPISA) process that allowed to readily produce stable, aqueous suspensions of mostly narrowly dispersed, degradable vinyl copolymer nanoparticles.



5. Reference

- [1] T. Safra, F. Muggia, S. Jeffers, D. Tsao-Wei, S. Groshen, O. Lyass, R. Henderson, G. Berry, A. Gabizon, *Annals of oncology : official journal of the European Society for Medical Oncology / ESMO* **2000**, *11*, 1029–1033.
- [2] P. Couvreur, C. Vauthier, *Pharmaceutical Research* **2006**, *23*, 1417–1450.
- [3] K. S. Soppimath, T. M. Aminabhavi, A. R. Kulkarni, W. E. Rudzinski, *Journal of Controlled Release* **2001**, *70*, 1–20.
- [4] W. B. Liechty, D. R. Kryscio, B. V Slaughter, N. A. Peppas, *Annual review of chemical and biomolecular engineering* **2010**, *1*, 149–173.
- [5] V. Delplace, J. Nicolas, *Nature Chemistry* **2015**, *7*, 771–784.
- [6] A. Tardy, J. Nicolas, D. Gigmes, C. Lefay, Y. Guillaneuf, *Chemical Reviews* **2017**, *117*, 1319–1406.

- [7] T. Pesenti, J. Nicolas, *ACS Macro Letters* **2020**, *9*, 1812–1835.
- [8] J. M. Siebert, D. Baumann, A. Zeller, V. Mailänder, K. Landfester, *Macromolecular Bioscience* **2012**, *12*, 165–175.
- [9] N. J. W. Penfold, J. Yeow, C. Boyer, S. P. Armes, *ACS Macro Letters* **2019**, *8*, 1029–1054.
- [10] N. J. Warren, S. P. Armes, *Journal of the American Chemical Society* **2014**, *136*, 10174–10185.
- [11] S. L. Canning, G. N. Smith, S. P. Armes, *Macromolecules* **2016**, *49*, 1985–2001.
- [12] P. Gurnani, C. P. Bray, R. A. E. Richardson, R. Peltier, S. Perrier, *Macromolecular Rapid Communications* **2019**, *40*, 1800314.
- [13] W.-J. Zhang, C.-Y. Hong, C.-Y. Pan, *Macromolecules* **2014**, *47*, 1664–1671.
- [14] N. J. Warren, O. O. Mykhaylyk, A. J. Ryan, M. Williams, T. Doussineau, P. Dugourd, R. Antoine, G. Portale, S. P. Armes, *Journal of the American Chemical Society* **2015**, *137*, 1929–1937.
- [15] C. Gonzato, M. Semsarilar, E. R. Jones, F. Li, G. J. P. Krooshof, P. Wyman, O. O. Mykhaylyk, R. Tuinier, S. P. Armes, *Journal of the American Chemical Society* **2014**, *136*, 11100–11106.
- [16] N. J. W. Penfold, J. R. Whatley, S. P. Armes, *Macromolecules* **2019**, *52*, 1653–1662.
- [17] D. B. Wright, M. A. Touve, L. Adamiak, N. C. Gianneschi, *ACS Macro Letters* **2017**, *6*, 925–929.
- [18] V. Delplace, S. Harrisson, A. Tardy, D. Gigmes, Y. Guillaneuf, J. Nicolas, *Macromolecular Rapid Communications* **2014**, *35*, 484–491.
- [19] G. Wang, M. Schmitt, Z. Wang, B. Lee, X. Pan, L. Fu, J. Yan, S. Li, G. Xie, M. R. Bockstaller, K. Matyjaszewski, *Macromolecules* **2016**, *49*, 8605–8615.
- [20] Y. Sha, M. A. Rahman, T. Zhu, Y. Cha, C. W. McAlister, C. Tang, *Chemical Science* **2019**, *10*, 9782–9787.
- [21] S. Varlas, J. C. Foster, P. G. Georgiou, R. Keogh, J. T. Husband, D. S. Williams, R. K. O'Reilly, *Nanoscale* **2019**, *11*, 12643–12654.
- [22] X. Wang, S. Man, J. Zheng, Z. An, *ACS Macro Letters* **2018**, *7*, 1461–1467.
- [23] J. Yeow, O. R. Sugita, C. Boyer, *ACS Macro Letters* **2016**, *5*, 558–564.
- [24] D. Le, F. Wagner, M. Takamiya, I.-L. Hsiao, G. Gil Alvaradejo, U. Strähle, C. Weiss, G. Delaittre, *Chemical Communications* **2019**, *55*, 3741–3744.
- [25] Y. Ding, Q. Zhao, L. Wang, L. Huang, Q. Liu, X. Lu, Y. Cai, *ACS Macro Letters* **2019**, *8*, 943–946.
- [26] S. Dong, W. Zhao, F. P. Lucien, S. Perrier, P. B. Zetterlund, *Polymer Chemistry* **2015**, *6*, 2249–2254.
- [27] C. A. Figg, A. Simula, K. A. Gebre, B. S. Tucker, D. M. Haddleton, B. S. Sumerlin, *Chemical Science* **2015**, *6*, 1230–1236.

- [28] J. Yeow, J. Xu, C. Boyer, *ACS Macro Letters* **2015**, *4*, 984–990.
- [29] B. Karagoz, L. Esser, H. T. Duong, J. S. Basuki, C. Boyer, T. P. Davis, *Polymer Chemistry* **2014**, *5*, 350–355.
- [30] W. Zhao, H. T. Ta, C. Zhang, A. K. Whittaker, *Biomacromolecules* **2017**, *18*, 1145–1156.
- [31] W.-J. Zhang, C.-Y. Hong, C.-Y. Pan, *Biomacromolecules* **2016**, *17*, 2992–2999.
- [32] W.-J. Zhang, C.-Y. Hong, C.-Y. Pan, *Macromolecular Rapid Communications* **2019**, *40*, 1800279.
- [33] L. D. Blackman, S. Varlas, M. C. Arno, A. Fayter, M. I. Gibson, R. K. O'Reilly, *ACS Macro Letters* **2017**, *6*, 1263–1267.
- [34] S. Kaga, N. P. Truong, L. Esser, D. Senyschyn, A. Sanyal, R. Sanyal, J. F. Quinn, T. P. Davis, L. M. Kaminskas, M. R. Whittaker, *Biomacromolecules* **2017**, *18*, 3963–3970.
- [35] V. Ladmiral, M. Semsarilar, I. Canton, S. P. Armes, *Journal of the American Chemical Society* **2013**, *135*, 13574–13581.
- [36] C. Gazon, P. Salas-Ambrosio, E. Ibarboure, A. Buol, E. Garanger, M. W. Grinstaff, S. Lecommandoux, C. Bonduelle, *Angewandte Chemie International Edition* **2020**, *59*, 622–626.
- [37] E. Guégain, C. Zhu, E. Giovanardi, J. Nicolas, *Macromolecules* **2019**, *52*, 3612–3624.
- [38] C. Zhu, J. Nicolas, *Polymer Chemistry* **2021**, *12*, 594–607.
- [39] F. M. Veronese, *Biomaterials* **2001**, *22*, 405–417.
- [40] F. Veronese and J.M. Harris, *Advanced Drug Delivery Reviews* **2002**, *54*, 453–456.
- [41] M. J. Roberts, M. D. Bentley, J. M. Harris, *Advanced Drug Delivery Reviews* **2002**, *54*, 459–476.
- [42] R. Duncan, *Nature Reviews Drug Discovery* **2003**, *2*, 347–360.
- [43] J. M. Harris, R. B. Chess, *Nature Reviews Drug Discovery* **2003**, *2*, 214–221.
- [44] J. Tran, E. Guégain, N. Ibrahim, S. Harrisson, J. Nicolas, *Polymer Chemistry* **2016**, *7*, 4427–4435.
- [45] E. Guégain, J. Tran, Q. Deguettes, J. Nicolas, *Chemical Science* **2018**, *9*, 8291–8306.
- [46] S. Stolnik, L. Illum, S. S. Davis, *Advanced Drug Delivery Reviews* **1995**, *16*, 195–214.
- [47] R. Gref, Y. Minamitake, M. T. Peracchia, V. Trubetskoy, V. Torchilin, R. Langer, *Science* **1994**, *263*, 1600–1603.
- [48] G. Storm, S. O. Belliot, T. Daemen, D. D. Lasic, *Advanced Drug Delivery Reviews* **1995**, *17*, 31–48.
- [49] E. Malikmammadov, T. E. Tanir, A. Kiziltay, V. Hasirci, N. Hasirci, *PCL and PCL-Based Materials in Biomedical Applications*, Taylor & Francis, **2018**.
- [50] M. R. Hill, E. Guégain, J. Tran, C. A. Figg, A. C. Turner, J. Nicolas, B. S. Sumerlin, *ACS Macro Letters* **2017**, *6*, 1071–1077.

- [51] E. Dalgakiran, H. Tatlipinar, *Physical Chemistry Chemical Physics* **2018**, *20*, 15389–15399.
- [52] V. Delplace, A. Tardy, S. Harrison, S. Mura, D. Gigmes, Y. Guillaneuf, J. Nicolas, *Biomacromolecules* **2013**, *14*, 3769–3779.
- [53] J. Tran, T. Pesenti, J. Cressonnier, C. Lefay, D. Gigmes, Y. Guillaneuf, J. Nicolas, *Biomacromolecules* **2019**, *20*, 305–317.